


Analytical model for the thermal resistance of windings consisting of solid or litz wire

Conference Paper**Author(s):**

Jaritz, Michael; Biela, Jürgen 

Publication date:

2013

Permanent link:

<https://doi.org/10.3929/ethz-b-000073291>

Rights / license:

[In Copyright - Non-Commercial Use Permitted](#)

Originally published in:

<https://doi.org/10.1109/EPE.2013.6634624>

Analytical model for the thermal resistance of windings consisting of solid or litz wire

Michael Jaritz, Juergen Biela
 Laboratory for High Power Electronic Systems, ETH Zuerich
 Email: jaritz@hpe.ee.ethz.ch
 URL: <http://www.hpe.ee.ethz.ch>

Keywords

<<Thermal resistance>>, <<Thermal model>>, <<Litz wire>>, <<Round wire>>

Abstract

In this paper a method to calculate the thermal resistance of windings is presented and validated by measurements. Two formulas have been developed for widely used wire types in power electronics being round and litz wire. With the presented approach it is possible to describe the thermal resistance of arbitrary wire arrangements. This analytical approach can either be used in fast forward designs of magnetic devices, respectively can also be integrated in automatized optimization procedures to improve the designs of magnetic components. The calculated results are showing good coincidence with the measured values.

Introduction

In almost every converter the design of magnetic components is an important part of the overall design. Due to the high number of degrees of freedom and geometric parameters this is often performed with the help of optimization procedures (see Fig.1(a))[1]. At the end of every design of a magnetic component the final component temperature is the constraint if the design is valid or the geometry has to be modified by the optimizer. Therefore, to obtain the temperatures in each part of the magnetic component, thermal

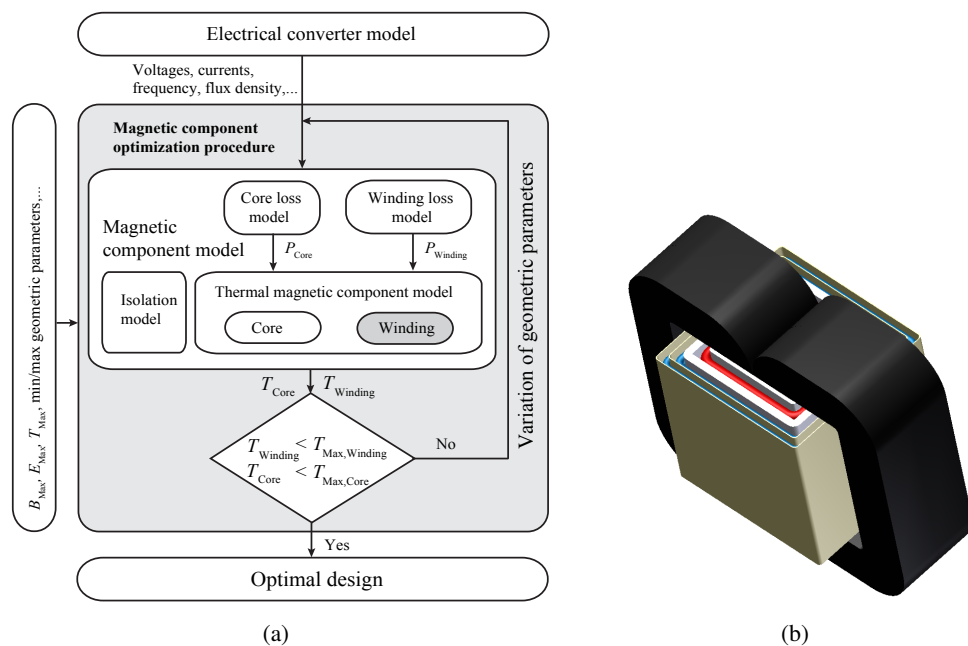


Figure 1: (a) General magnetic component optimization procedure. (b) Optimized transformer geometry.

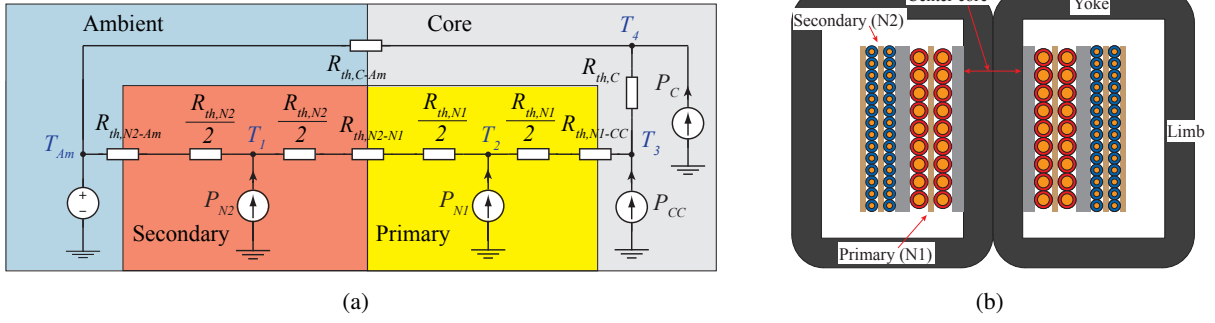


Figure 2: (a) Thermal equivalent circuit of a transformer. (b) Cross section of the transformer in Fig. 1(b).

equivalent circuits are used. Based on the transformer thermal model (e.g.[1]), all critical temperatures are determined (see Fig.2(a)). The model contains all types of heat transfers represented by equivalent thermal resistors and all losses are modelled by current sources. In Fig.2(b) the thermal transition between core parts and windings ($R_{th,N1-CC}$), the heat transfer within the core ($R_{th,C}$) respectively between primary and secondary winding ($R_{th,N1-N2}$) is performed by heat conduction. Also the heat transfer within the windings ($R_{th,Nx}$) is represented by this type of heat transfer. The thermal resistances between core and ambient ($R_{th,C-Am}$) or winding and ambient ($R_{th,N2-Am}$) are based on radiation and convection. Most of before mentioned thermal resistors are well described in literature e.g. [2], but there exists a lack concerning the accurate determination of the thermal winding resistance $R_{th,Nx}$. Either there is the use of strongly simplified approximation formulas [3],[4],[5] where the transition between single wires and winding layers is neglected, or the resistance is modelled with the help of measurements [6],[7] or finite element method (FEM) [8],[9]. This paper presents an analytical expression for the thermal winding resistor $R_{th,Nx}$ which can be used within optimization algorithms for transformer or inductance design. The derivation of $R_{th,Nx}$ is given in detail in section II. In section III, a measurement setup to verify the results of section II is presented. Finally, the results from calculation and measurement are compared in section IV.

Derivation of the thermal resistance

To describe thermal transitions in transformer or inductance windings it is necessary to describe the way of the heat flow \dot{Q} . This way can be represented by a thermal resistance $R_{th,Nx}$ which is derived in this section. The thermal resistance $R_{th,Nx}$ is formed by a parallel connection of a tangential resistance $R_{th,tan}$ and a radial part $R_{th,rad}$. The calculation of the tangential part is presented in a first step. The radial part is based on an electrothermal analogy as will be explained thereafter.

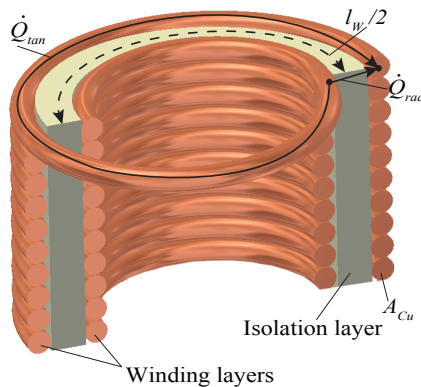


Figure 3: Heat flow in multiple layer windings.

Tangential thermal resistance

The heat flow \dot{Q} in multiple layer windings can be divided into two shares [10] (see Fig. 3). First, in a tangential part \dot{Q}_{tan} which takes the flow along the winding from layer to layer into account. Second, in a radial part \dot{Q}_{rad} which represents the heat flow between two neighbouring winding layers through the isolation layer. The tangential part between two corresponding winding layers $R_{th,tan}$ can be calculated by

$$R_{th,tan} = \frac{l_W \cdot (2N_{pL} - 1)}{2\lambda_{Cu}A_{Cu}} \approx \frac{l_W \cdot N_{pL}}{\lambda_{Cu}A_{Cu}} \quad (1)$$

where N_{pL} is the number of turns per layer, l_W is the mean length per turn and A_{Cu} the copper cross section.

Electrothermal analogy

In literature, the electrothermal analogy is often described with the help of the electrical flow field and the thermal flow field which leads to the thermal circuit model depicted in Fig.2 [11]. Another analogy is between the electrostatic field and the thermal flow field. There, the electrical field lines can be regarded as the heat flow lines in a thermodynamic problem. All relations between these analogies are listed in Tab.I.

Basic winding arrangements can be divided into orthogonal arranged wires (see Fig.4) and orthocyclic arranged wires (see Fig.5). In orthogonal windings, the wires of the second layer are lying exactly on top or beside the next layer, whereas in orthocyclic windings the wires of the next layer are lying in the gaps of the previous layer. Fig.4(b) shows the electrical field distribution between two orthogonal arranged wires, each with different potential p_1 , p_2 on an equipotential surface. The thermal flow field distribution is shown in Fig.4(c). There, the conductor surface is approximately an isothermal surface with given temperatures T_1 , T_2 . Comparing Fig.4 (b) and (c) shows a good match of the electrical and the thermal field lines. Hence, the calculation of the radial thermal resistance $R_{th,rad}$ between two round orthogonal arranged conductors is based on the calculation of the electrical capacitance between two of them as presented in [12]. For the sake of completeness, the derivation of the electrical capacitance is shortly summarized at first and in a second step, the transition to the thermal resistance is given.

Orthogonal winding capacitance model

To derive the orthogonal winding capacitance model, two wires are arranged next to each other, separated by an isolation layer (see Fig. 4(a)). In a first assumption, it can be stated that the electrical field lines will have almost no deviation in the isolation layer because in most cases the isolation layer of the wire with the thickness δ is much smaller than the radius r_o of the wire and the deviation of the E-field lines due to the different permittivities of copper and the isolation can be neglected. Finally, the field lines run through the isolation layer h perpendicularly. Comparing Fig. 4 (a) and (b), the deviations of the field lines have their maximum at $\varphi = 0$ and a minimum at $\varphi = \pi/2$. Due to the fact that most of the field lines will run in the region of $\varphi = \pi/2$, the error is low. The derivation is given in the following.

According to the boundary conditions between wire isolation and air follows

$$\varepsilon_{Iso}E_{Iso} = E_{Air} \sin \varphi \quad (2)$$

Where ε_{Iso} is the permittivity and E_{Iso} the electrical field strength of the wire isolation. E_{Air} is the field strength in air. The perpendicular ingress of the field lines from air into the isolation layer leads to

$$\varepsilon_{Lay}E_{Lay} = E_{Air} \quad (3)$$

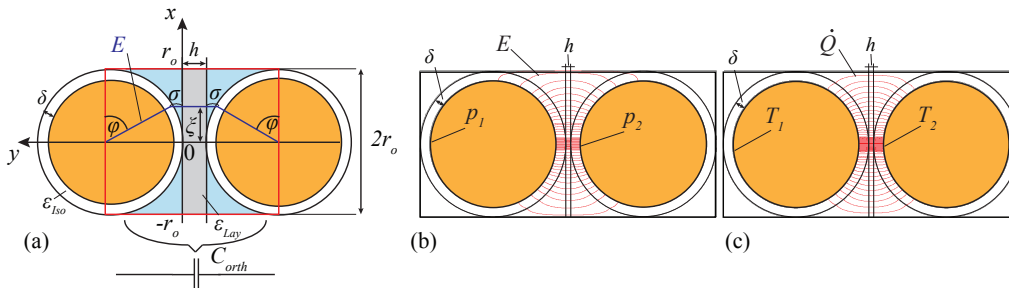


Figure 4: (a) Two orthogonal arranged wires with ideal assumed electrical field lines. (b) Electrical field lines between two wires with potential p_1 and p_2 . (c) Thermal heat flow between two wires simulated with COMSOL.

Table I: Electrothermal analogy

Electrostatic field		Electrical flow field		Thermal flow field	
Charge	Q	Current	I	Heat flow	\dot{Q}
Capacitance	C	Conductance	G	Thermal conductance	G_{th}
Voltage	V	Voltage	V	Temperature difference	ΔT
Permittivity	ϵ	Specific conductivity	γ	Thermal conductivity	λ
$Q = C \cdot V$		$I = G \cdot V$		$\dot{Q} = G_{th} \cdot \Delta T$	

where ϵ_{Lay} is the permittivity and E_{Lay} is the electrical field strength of the isolation layer. Performing the line integral of the voltage between the two conductors gives

$$V = 2E_{Iso}\delta + E_{Lay}h + 2E_{Air}\sigma \quad . \quad (4)$$

Using (2), (3), (4) and introducing

$$\sin\varphi = \frac{\sqrt{r_o^2 - \xi^2}}{r_o} \quad \text{and} \quad \sigma = r_o - \sqrt{r_o^2 - \xi^2} \quad (5)$$

and by substituting

$$\alpha = 1 - \frac{\delta}{\epsilon_{Iso}r_o} \quad \text{and} \quad \beta = \frac{1}{\alpha} \left(1 + \frac{h}{2\epsilon_{Lay}r_o} \right) \quad (6)$$

all field strengths can be calculated by

$$E_{Lay} = \frac{V}{2\epsilon_{Lay}\alpha \left(\beta r_o - \sqrt{r_o^2 - \xi^2} \right)}, \quad E_{Iso} = \frac{V\sqrt{r_o^2 - \xi^2}}{2\epsilon_{Iso}r_o\alpha \left(\beta r_o - \sqrt{r_o^2 - \xi^2} \right)}, \quad E_{Air} = \frac{V}{2\alpha \left(\beta r_o - \sqrt{r_o^2 - \xi^2} \right)}. \quad (7)$$

The different energy contributions are belonging to the area in the red rectangle (see Fig. 4(a)). The energy in the isolation layer is

$$W_{Lay} = \frac{\epsilon_o\epsilon_{Lay}lWh}{2} \int_{-r_o}^{+r_o} E_{Lay}(\xi)^2 d\xi \quad . \quad (8)$$

The energy in the wire isolation in polar coordinates with the origin in the center of the left wire is

$$W_{Iso} = \epsilon_o\epsilon_{Lay}lW \int_0^\pi \int_{r_o - \frac{\delta}{2}}^{+r_o} E_{Iso}(\varphi)^2 r dr d\varphi \quad (9)$$

and the energy in the air in cartesian coordinates

$$W_{Air} = \epsilon_o lW \int_{-r_o}^{+r_o} \int_0^{\sigma(x)} E_{Air}(x,y)^2 dy dx \quad . \quad (10)$$

The total energy then is formed by

$$W_{all} = W_{Lay} + W_{Iso} + W_{Air} \quad . \quad (11)$$

After solving the integrals and several steps of substitution,

$$W_{all} = \frac{\epsilon_o lW V^2}{\alpha} \left\{ Y + \frac{1}{8\epsilon_{Iso}} \left(\frac{2\delta}{r_o} \right)^2 \frac{Z}{\alpha} \right\} \quad (12)$$

with

$$Y = \arctan \left(\sqrt{\frac{\beta+1}{\beta-1}} \right) \frac{\beta}{\sqrt{\beta^2-1}} - \frac{\pi}{4} \quad (13)$$

and

$$Z = \frac{\beta (\beta^2 - 2)}{(\beta^2 - 1)^{3/2}} \arctan \left(\sqrt{\frac{\beta + 1}{\beta - 1}} \right) - \frac{\beta}{2\beta^2 - 2} - \frac{\pi}{4} \quad (14)$$

The capacitance can be found by comparison of coefficients (12) with $W = C_{orth}V^2/2$ which leads to

$$C_{orth} = \frac{2\epsilon_o l W}{\alpha} \left\{ Y + \frac{1}{8\epsilon_{Iso}} \left(\frac{2\delta}{r_o} \right)^2 \frac{Z}{\alpha} \right\} \quad (15)$$

The transition to the thermal resistance follows below.

Orthocyclic winding capacitance model

In case of orthocyclic layers, the basic capacitance describes the energy which is stored between the two neighbouring wires in the left layer and the one wire in the right layer as shown in the basic cell, which is a triangle in Fig.5(a). Its energy has to be multiplied by two considering also the energy in both of the adjacent triangles which are also contributing to the entire energy of the basic capacitance. Again, the trends of the electrical and thermal flux lines depicted in Fig. 5 (b) and (c) showing good accordance like in the orthogonal case. Taking the same assumptions into account for the electrical field lines like in the orthogonal case leads to [12]:

$$C_{cyc} = 4\epsilon_o l W \left[M_{Air} + M_{Iso} \left(\frac{\delta}{\epsilon_D r_o^2} \right) \left(r_o - \frac{\delta}{2} \right) \right] \quad (16)$$

with

$$M_{Air} = \int_0^{\frac{\pi}{6}} \frac{\cos^2 \psi - \cos \psi \sqrt{\cos^2 \psi - 0.75} - 0.5}{\left[\cos \psi - \alpha (\sqrt{\cos^2 \psi - 0.75} + 0.5) \right]^2} d\psi \quad (17)$$

$$M_{Iso} = \int_0^{\frac{\pi}{6}} \frac{\sin^2 \psi + \cos \psi \sqrt{\cos^2 \psi - 0.75}}{\left[\cos \psi - \alpha (\sqrt{\cos^2 \psi - 0.75} + 0.5) \right]^2} d\psi \quad (18)$$

In the following, the transition to the thermal resistance is described next.

Radial thermal resistance

In order to determine the radial thermal resistance, the analogy between the electrostatic field and the thermal flow field from Tab. I is applied. By simply replacing all permittivities with the equivalent thermal conductivities and building the inverse of (15) and (16), $R_{th,rad}$ can be obtained as

$$R_{th,rad,orth} = \left[\frac{2\lambda_{Air} l W}{\alpha} \left(Y + \frac{1}{8\lambda_{Iso}/\lambda_{Air}} \left(\frac{2\delta}{r_o} \right)^2 \frac{Z}{\alpha} \right) \right]^{-1} \quad (19)$$

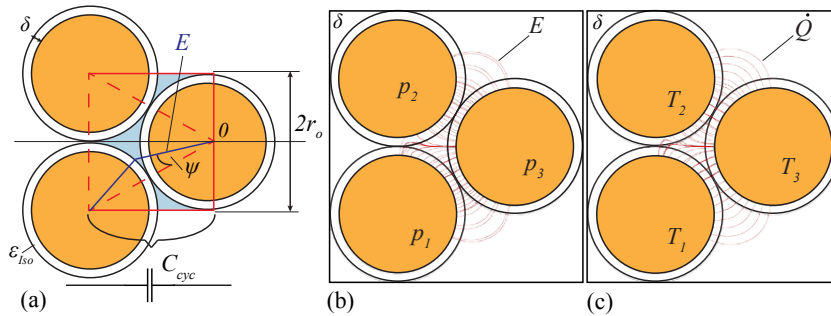


Figure 5: (a) Three orthocyclic arranged wires with ideal assumed electrical field lines and basic cell (dotted triangle). (b) Electrical field lines between three orthocyclic arranged wires with potentials p_1 , p_2 and p_3 . (c) Thermal heat flow between three orthocyclic arranged wires simulated with COMSOL.

and

$$R_{th,rad,cyc} = \left[4\lambda_{Air}l_W \left(M_{Air} + M_{Iso} \left(\frac{\delta}{\lambda_{Iso}/\lambda_{Air}r_o^2} \right) \left(r_o - \frac{\delta}{2} \right) \right) \right]^{-1} \quad (20)$$

with

$$\epsilon_o \circ \bullet \lambda_{Air} \quad \epsilon_{Lay} \circ \bullet \frac{\lambda_{Lay}}{\lambda_{Air}} \quad \epsilon_{Iso} \circ \bullet \frac{\lambda_{Iso}}{\lambda_{Air}} \quad (21)$$

Where λ_{Air} is the thermal conductivity of air, λ_{Lay} the conductivity of the isolation layer and λ_{Iso} is the conductivity of the wire isolation.

Finally, in case of an either pure orthogonal or orthocyclic winding the final thermal resistance can be written as

$$R_{th,Nx} = (R_{th,tan} || R_{th,rad}) \frac{N_L}{N_{pL}} \quad (22)$$

For simplification reasons $R_{th,rad,orth}$ and $R_{th,rad,cyc}$ are renamed to $R_{th,orth}$ and $R_{th,cyc}$. In general every winding is a combination of both thermal radial resistances and will be investigated in the next section.

Combined thermal resistance and split resistor model of round solid wire windings

Due to manufacturing reasons the overall thermal resistance $R_{th,Nx}$ of a solid wire winding as shown for example in Fig 6(a) is a combination of an orthogonal and an orthocyclic wire arrangement. Usually, at least both halves of the outer layers of the winding can be regarded as one orthogonal layer (see Fig.7(a) and (b)). This leads to the general form

$$R_{th,Nx} = (R_{th,tan} || R_{th,cyc}) \frac{N_L - N_{orth}}{N_{pL}} + (R_{th,tan} || R_{th,orth}) \frac{N_{orth}}{N_{pL}} \quad (23)$$

where N_{orth} is the number of considered orthogonal layers.

Fig. 6(b) shows the transition from a winding with single solid copper wires and combined layers to a split model with $R_{th,Nx}$ which is used in Fig.2 to model the winding.

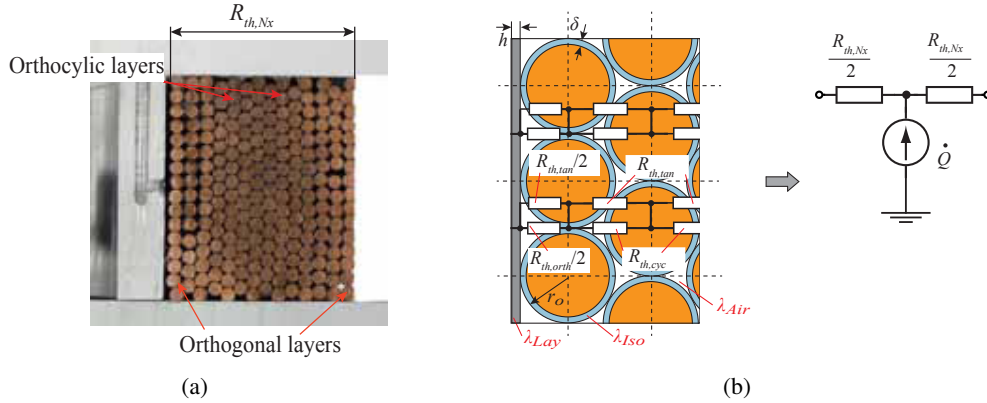


Figure 6: (a) Cross section of a solid wire winding with orthogonal and orthocyclic layers. (b) Transition from the physical solid wire winding with combined layers to the split resistor model.

Combined thermal resistance and split resistor model of litz wire windings

As litz wire is often used to reduce high frequency losses in windings, the analytical model for litz wire is presented in the following. Fig.7(a) shows the cross section of a litz wire winding with three orthocyclic layers and one orthogonal layer. The transition from the physical litz wire winding to the thermal split model is shown in Fig.7(b) and can be performed in 3 steps. Step (A) starts with the transformation of the round litz wire bundle with N_S strands into a square litz bundle with side length $\sqrt{N_S} \cdot 2r_o$. In step (B), the resistance between each litz bundle is calculated and finally in step (C) this leads to the split model. One way to model the thermal resistance of the litz wire bundle $R_{th,Litz}$ is the series connection

of the orthocyclic contributions $R_{th,L,cyc}$ between each litz strand and the orthogonal part $R_{th,L,orth}$ at the edges (see Fig.7(b)). Both resistors are determined by using litz strand parameters and (20) for $R_{th,L,cyc}$ and (19) for $R_{th,L,orth}$. Finally

$$R_{th,Litz} = R_{th,L,cyc} \left(1 - \frac{1}{\sqrt{N_S}} \right) + \frac{R_{th,L,orth}}{\sqrt{N_S}} \quad (24)$$

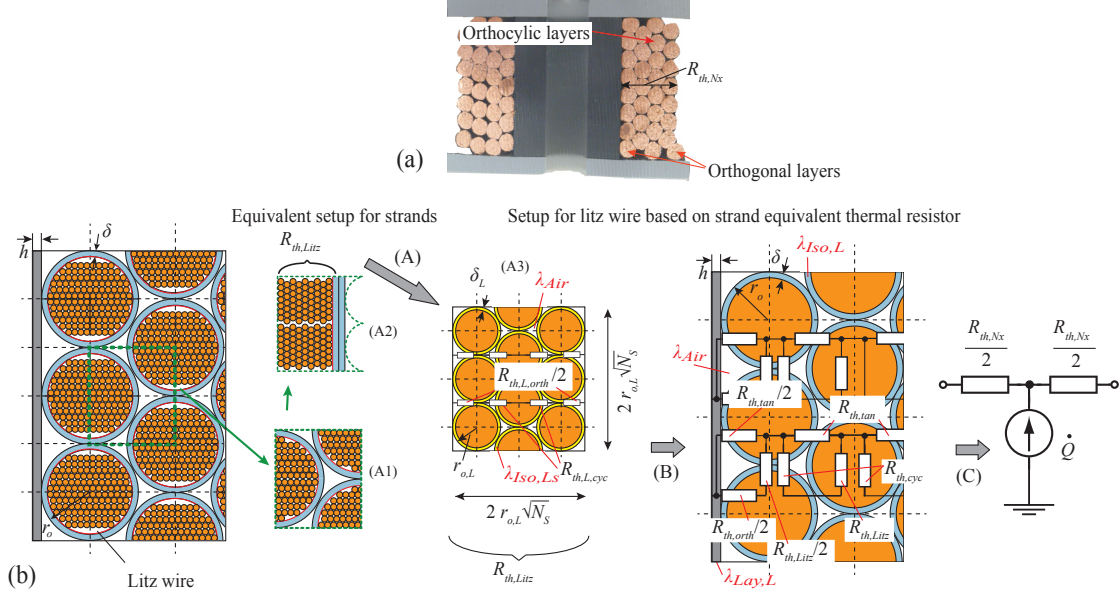


Figure 7: (a) Cross section of a litz wire winding. (b) Transition from the round litz wire bundle into a square litz bundle (A). There, the litz strands of the dotted green square (A1) are rearranged to a squared pattern and the outer isolation is shifted to the right (A2). (A3) shows the thermal network of one rearranged litz bundle. Calculation of the thermal resistance between each bundle (B), leads to a split thermal resistor model (C) of the whole litz winding.

An extended model of the litz wire bundle is depicted in Fig.8. There, the heat flow is modelled by the already known radial part $\dot{Q}_{rad,L}$ and in addition a part along a single litz strand \dot{Q}_{SL} caused by the lay. There exists also a tangential contribution, but due to the high ratio between mean length per turn and litz strand cross section it can be neglected. The way along the strand can be described by

$$R_{th,SL} = \frac{SL/2}{\lambda_{Cu} r_o^2 \pi} \quad (25)$$

where SL is the lay length of the litz wire and results in the network shown in Fig.8(b). Solving this network with a program like PSPICE gives $R'_{th,Litz}$. This thermal resistor represents one horizontal layer

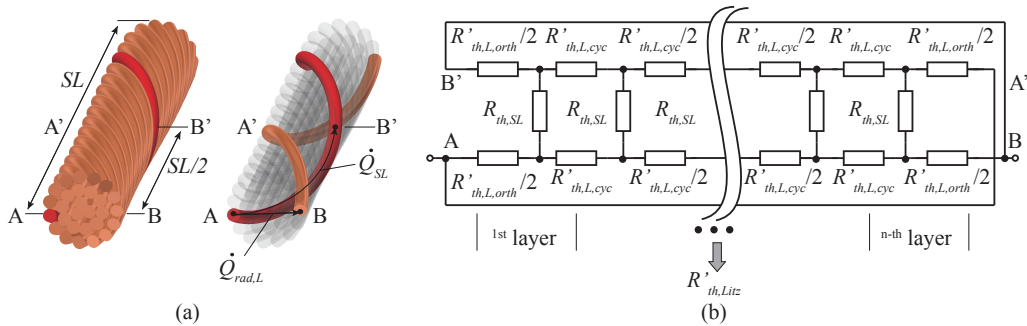


Figure 8: (a) Litz wire with two considered heat paths $\dot{Q}_{rad,L}$ and \dot{Q}_{SL} . (b) Equivalent thermal network of one horizontal litz strand layer from A to B and A' to B'.

of litz wires from point A to B and from point A' to B'. Due to this parallel path, the resulting resistor $R'_{th,Litz}$ has to be divided by $\sqrt{N_S} \cdot l_W \cdot 0.5$. Additionally the resistors $R_{th,L,orth}$ (litz strand parameters and (19)) and $R_{th,L,cyc}$ (litz strand parameters and (20)) have to be multiplied by l_W .

$$R_{th,Litz} = \frac{2R'_{th,Litz}}{\sqrt{N_S}l_W} \quad \text{with} \quad R'_{th,L,cyc} = l_W R_{th,L,cyc} \quad \text{and} \quad R'_{th,L,orth} = l_W R_{th,L,orth} \quad (26)$$

Finally using (24) or (26) with litz strand parameters and (1), (19), (20) with litz bundle parameters gives the general form of the thermal resistance of litz wire windings as

$$R_{th,Nx} = [R_{th,tan} || (R_{th,cyc} + R_{th,Litz})] \frac{N_L - N_{orth}}{N_{pL}} + [R_{th,tan} || (R_{th,orth} + R_{th,Litz})] \frac{N_{orth}}{N_{pL}} \quad (27)$$

Measurement setup

For validating the models depicted in Fig.6 and Fig.7 two test setups as shown in Fig.9 have been built. Three plastic layers are used for thermal isolation through which a negligible amount of heat is dissipated and the generated heat will be forced to dissipate in y-direction through the winding. The inner isolation layer is made of PET because this material withstands continuous temperatures up to 100°C but unfortunately has a relatively high thermal conductivity. To overcome this problem two additional layers of PVC are attached on the top and bottom respectively.

Two power resistors are employed as heat sources mounted on an aluminium tube which is also used as the winding bobbing. In the first case, the test windings consists of 14 winding layers N_L and 16 turns per layer N_{pL} . The wire is an enamelled round Cu-wire with PEI and PAI isolation. In the second case, litz wire is used to build a winding consisting of 10 winding layers N_L and 10 turns per layer N_{pL} . An polyesterfilm folie (Mylar®) is used for the outer isolation. To determine the inner and the outer winding temperature two temperature sensors (K-type thermo couples) are mounted as shown in Fig.9(a) and (b). All other material and geometric properties are listed in Tab. II. The photo of the test setup is shown in Fig. 9(b), once without the winding and with mounted heating resistor and once completely assembled.

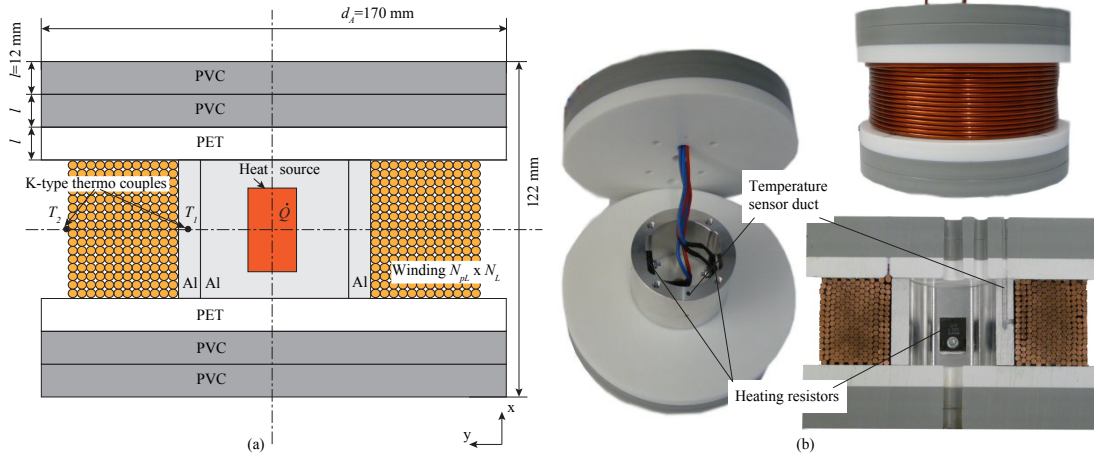


Figure 9: (a) Thermal test setup cross section. (b) Manufactured thermal test setup, here of single solid wire.

Results

The comparison between the measurements and the analytical model is given in the following for the single solid wire winding exemplarily (see Fig.9(b)).

Using (23) and the parameters from Tab.II results in $R_{th,Nx} = 2.06^\circ\text{C}/\text{W}$. Concerning that the isolation of the wire is a combination of a PEI and a PAI material the mean value of both of them will be used for the thermal conductivity λ_{Iso} . The thermal resistance in x-direction of the thermal isolation layer is

$$R_{th,PVC,PET} = 2(2R_{th,PVC} + R_{th,PET}) = 18.5^\circ\text{C}/\text{W} \quad \text{where} \quad R_{th,x} = \frac{4l}{d_A^2 \pi \lambda_x} \quad (28)$$

Table II: Material properties and winding parameters.

Material properties			
Material	Parameter	Thermal conductivity λ in W/Km	Max. continuous temperature T_{max} in C°
Air [13]	λ_{Air}	0.028	–
Copper (Cu) [13]	λ_{Cu}	401	~ 1000
Polyvenylchlorid (PVC) [14]	λ_X	0.15	60
Polyethylenterephthalat (PET) [14]	λ_X	0.24	100
Polyetherimid (PEI) [14]	λ_{Iso}	0.24	170
Polyurethan (PU,PUR) [14]	$\lambda_{Iso,LS}$	0.245	120
Polyamidimid (PAI) [15]	λ_{Iso}	0.26	250
Polyesterfilm (Mylar®) [16]	$\lambda_{Iso,L}$	0.155	< 200

Winding parameters		Round wire	Litz wire
		SH-Term 210 Grad 2 [17]	RUPALIT®Safety V155 [18]
r_o	[mm]	1.563	2.5
δ	[μm]	63	37.5
l_W	[mm]	357.4	377
h	[mm]	0	0
$r_{o,L}$	[μm]	–	50
δ_L	[μm]	–	4
SL	[mm]	–	47
N_S	–	–	1260
N_L	–	14	10
N_{pL}	–	16	10
N_{orth}	–	1,6	1

Due to the fact that the ratio between $R_{th,PVC,PET}$ and $R_{th,Nx}$ is about 9 the heat loss through the isolation layer can be neglected and the thermal setup will be described with the simplified thermal circuit as shown in Fig. 10. The $R_{th,Nxm}$ from measurements can then be found by

$$R_{th,Nxm} = \frac{\Delta T}{\dot{Q}} = \frac{T_1 - T_2}{\dot{Q}} \quad . \quad (29)$$

Using $N_{orth} = 6$ (as given in Fig.6(a)) results in a low error between the calculated and the measured resistance in the case of round wire, as can be seen in Tab. III. Generally, the number of N_{orth} is not available, so the deviation for at least both halves of the outer layers which can be regarded as one

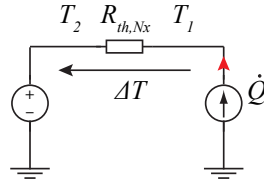


Figure 10: Simplified thermal equivalent circuit of the test setup.

Table III: Results

	Measured results			Calculated results		Used equ.	N_{orth}
	$\Delta T [^\circ C]$	$\dot{Q} [W]$	$R_{th,Nxm} [^\circ C/W]$	$R_{th,Nx} [^\circ C/W]$	Error [%]		
Round wire [17]	45.6	22.1788	2.06	1.6343	-20.7	(23)	1
				2.1124	+2.5	(23)	6
Litz wire [18]	52.6	20.98	2.51	3.9132	+55.9	(24),(27)	1
				3.757	+49.68	(25),(26),(27)	1

orthogonal layer ($N_{orth} = 1$) is also given below. The deviation in case of litz wire is higher. This can be explained by the fact that the analytical approach is assuming that the heat transition points towards the bobbin and between the wires are pure contact points, not as seen in Fig.7(a) some kind of contact areas. Therefore, the calculated resistance is too high.

Conclusions

In this paper, the derivation of the thermal resistance of multiple layer windings with single solid wires or litz wires has been presented and validated by measurements. This analytical approach can either be used in fast forward designs of magnetic devices, respectively can also be integrated in automatized optimization procedures. Replacing λ_{Air} by a corresponding thermal conductivity also moulded windings can be considered. The error between the analytical solution and measurements in the case of round wire is low. In the case of litz wire it is a worst case approximation.

Acknowledgement

The authors would like to thank the project partners CTI and Ampegon AG very much for their strong support of the CTI-research project 13135.1 PFFLR-IW.

References

- [1] M. Jaritz and J. Biela, "Optimal design of a series parallel resonant converter for a solid state long pulse modulator," 4th Euro-Asian Pulsed Power Conference, 2012.
- [2] I. Villar, *Multiphysical characterization of medium-frequency power electronic transformers*. PhD thesis, Ecole polytechnique federal de Lausanne, 2010.
- [3] R. Petkov, "Optimum design of a high-power, high-frequency transformer," *IEEE Transactions on Power Electronics*, vol. 11, no. 1, pp. 33–42, 1996.
- [4] E. Snelling, *Soft Ferrites - Properties and Applications*. PSMA Reprint, 2005.
- [5] T. Undeland, J. Lode, R. Nilssen, W. Robbins, and N. Mohan, "A simple noniterative procedure for designing naturally-cooled high-frequency inductors and transformers based upon limitation of the maximum device temperature," in *IEEE Industry Applications Society Conference Meeting*, pp. 1253–1260 vol.2, 1994.
- [6] W. Odendaal and J. Ferreira, "A thermal model for high-frequency magnetic components," *IEEE Transactions on Industry Applications*, vol. 35, no. 4, pp. 924–931, 1999.
- [7] M. Rascon, J. Ara, R. Madsen, J. Navas, M. Perez, and F. San Miguel, "Thermal analysis and modelling of planar magnetic components," in *16th IEEE Applied Power Electronics Conference and Exposition, (APEC)*, vol. 1, pp. 97–101, 2001.
- [8] J. Faiz, M. B. B. Sharifian, and A. Fakhri, "Two-dimensional finite element thermal modeling of an oil-immersed transformer," *European Transactions on Electrical Power*, vol. 18, no. 6, pp. 577–594, 2008.
- [9] C. Hwang, P. Tang, and Y. Jiang, "Thermal analysis of high-frequency transformers using finite elements coupled with temperature rise method," *IEE Proceedings on Electric Power Applications*, vol. 152, no. 4, pp. 832 – 836, 2005.
- [10] P. Wallmeier, *Automatisierte Optimierung von induktiven Bauelementen*. PhD thesis, Universität-GH Paderborn, 2001.
- [11] W. Polifke and J. Kopitz, *Wärmeübertragung*. Pearson Studium, 2009.
- [12] J. Koch, "Berechnung der Kapazität von Spulen, insbesondere in Schalenkernen," tech. rep., Valvo Berichte Band XIV Heft 3, 1968.
- [13] *VDI-Wärmeatlas*. Springer-Verlag Heidelberg Berlin, 2006.
- [14] "<http://www.kern-gmbh.de>."
- [15] "<http://www.khp-kunststoffe.de>."
- [16] "<http://www2.dupont.com>."
- [17] "<http://www.sh-elektrodraht.de>."
- [18] "<http://www.pack-feindraehnte.de>."